Experimental Thermal and Fluid Science 35 (2011) 319–327

Contents lists available at ScienceDirect

Experimental Thermal and Fluid Science

journal homepage: www.elsevier.com/locate/etfs

Wavelet analysis of unsteady flows: Application on the determination of the Strouhal number of the transient wake behind a single cylinder

Maria Luiza S. Indrusiak [1], Sergio Viçosa Möller *

PROMEC – Universidade Federal do Rio Grande do Sul, Rua Sarmento Leite, 425, 90.050-170, Porto Alegre, RS, Brazil

ARTICLE INFO

Article history:
Received 2 March 2010
Received in revised form 5 October 2010
Accepted 6 October 2010

Keywords:
Turbulent flow
Wavelet analysis
Fourier analysis
Transient wake

ABSTRACT

This paper presents experimental results of the accelerating and decelerating flow in the wake of a cylinder obtained by means of hot wire anemometry measurements in a wind tunnel with high blockage ratio. The analysis was done in Fourier and wavelet spaces. The Strouhal number for Reynolds numbers up to 3×10^4 was studied in a transient flow and compared with the results obtained from steady flows at several velocities uniformly distributed from $Re = 1.7 \times 10^3$ to 3×10^4. Results show that the wavelet analysis is a valuable tool to deal with both transient and stationary random phenomena and that is able to capture the characteristics of the transient flow as well as the Fourier analysis can do with the steady state acquisitions.

1. Introduction

The flow on cylinders and the wake formed behind them is of great interest and object of many research studies. Single cylinders as well as cylinder arrangements simulate a wide range of practical situations, e.g. transmission lines, offshore structures and more complex arrangements, like tube banks of shell and tube heat exchangers.

Many articles found in the literature are concerned to equipment integrity, due to the close relationship between fluid flow around a solid surface or a structural element and the vibrations induced by the flow in the structure.

In general, fluid flow loads on a structure can be classified in static and dynamic loads. The former, due to the mean pressure variation of the flow along the structure, the latter, associated to pressure and velocity fluctuations due to vortex shedding and to the turbulence in the flow.

The first article relating frequency (of aeolian tones) and velocity of the flow over a bluff body was written by Čeněk (Vincenc) Strouhal in 1878 [1]. Since 1908, with the works performed by Bénard [2,3], studies of vortex shedding are found in the literature, with focus on the behavior of the wake of a single cylinder or two or more cylinders in steady state [4–9].

Unsteady flow results of flow visualization using Laser Induced Photochemical Anemometry are presented by Chu and Liao [10] for a Reynolds number range from 500 to 3000. Authors made also a comprehensive literature review.

Experimental results in turbulence are usually characterized by their mean values and through Fourier analysis, which provide information about the behavior of steady state phenomena in the frequency domain. This is not the case of field measurements, extreme situation of which would be the case of typhoon winds [11,12]. In transient flows, besides the variable mean values, additional phenomena may appear, as the flow velocity changes with time.

Steady state phenomena are a particular case of the transient general rule in nature. In engineering applications the steady state assumption is very useful and feasible in most situations. Nonetheless, in some situations a steady state approach may leave unnoticed some features of the phenomena.

Wavelets are valuable tools to analyze non-stationary time series and their possible singularities [13]. Wavelet transforms were used in applications such as presented in [14], to investigate the turbulence homogeneity at several scales, or to obtain power and cross spectrum, as in [15,16] or to detect coherent structures [17]. The orthonormal wavelet representation in experimental and numerical flow data sets was presented in [18]. Attention was given to single point measurements in steady state flow of a wake and a boundary layer to underline the capability of wavelets to demonstrate the intermittence in the smallest scales. For the interpretation of switching flows, wavelet analysis in addition to Fourier analysis was used [19,20]. Wavelet transforms were also used to study the vorticity structure in the far wake downstream of a cylinder [21,22], transient phenomena in tube banks [23] and the bistable flows in tube banks [24].

* Corresponding author.
E-mail address: svmoller@ufrgs.br (S.V. Möller).
[1] Present address: Universidade do Vale do Rio dos Sinos, São Leopoldo, RS, Brazil.

0894-1777 © 2010 Elsevier Inc. Open access under the Elsevier OA license.
doi:10.1016/j.expthermflusci.2010.10.001

Nomenclature

a	scale wavelet coefficient
b	position wavelet coefficient
CWT	continuous wavelet transform
D	diameter – m
DWT	discrete wavelet transform
DWPT	discrete wavelet packet transform
f	frequency – Hz
$\bar{f}(t)$	mean frequency of the interval – Hz
Fs	sampling frequency – Hz
F_ψ	pseudo frequency of the wavelet
j, J	scale coefficients of the DWT and DWPT
k	position coefficient of the DWT and DWPT
m	modulation parameter of the DWPT
$P_{xx}(f)$	Fourier spectrum
$P_{xx}(a,b)$	continuous wavelet spectrum
$P_{xx}(j,k)$	discrete wavelet spectrum
$P_{xx}(j,m,k)$	discrete wavelet packet spectrum
Re	Reynolds number ($U D/v$)
S	Strouhal number ($f D/U$)
$S(t)$	transient Strouhal number
t	time – s
U	velocity – m/s
Ua	approaching velocity – m/s
$x(t)$	generic function in time domain
$x(f)$	generic function in Fourier domain
$\tilde{X}(a,b)$	generic function in wavelet domain (continuous)
$\tilde{X}(j,m,k)$	generic function in wavelet domain (discrete, packet)
$\tilde{X}(j,k)$	generic function in wavelet domain (discrete)
$\psi(t)$	generic wavelet function

Most articles about flow on bluff-bodies consider an infinite domain, but in many cases it is important to take into account the effect of the blockage ratio. Ref. [25] presents the study of the blockage effect on the Strouhal number of a cylinder wake for Reynolds numbers between 10^4 and 10^5. Authors show that, for blockage ratios higher than 6% there is a distinct distortion of the flow field, with complex effects that made unsuitable a correction method. The confined flow around rectangular cylinders at various Reynolds numbers and blockage ratios is presented in [26] showing that the Strouhal number and the drag coefficient increase with the blockage ratio. The effect is more pronounced at lower Reynolds numbers.

In numerical studies, the computational domain is restricted in order to reduce the computational time and hardware requirements. This introduces numerical blockage effects as shown in [27], where the numerical blockage effects on steady and unsteady wake of a circular cylinder at Re = 106 and blockage ratios of 5%, 15% and 25% is studied. Results show that the hydrodynamic forces on the cylinder and the Strouhal number are magnified as the blockage ratio increases.

The purpose of this paper is to investigate the use of wavelets applied to the analysis of transient signals. The chosen problem is the well known wake behind a single cylinder submitted to a flow. The wavelet results for hot wire anemometry signals on accelerating and decelerating wakes are compared to Fourier results obtained from series of measurements of steady state flows up to a Reynolds number of 3×10^4. The effect of the blockage ratio, in this case, 16.5%, will also be discussed.

2. Background

The Fourier transform of a discrete time series representing a finite function $x(t)$ enables the study of the bulk spectral behavior of the random phenomenon represented by the series and is defined as:

$$\hat{x}(f) = \frac{1}{2\pi} \sum x(t) e^{-ift} \tag{1}$$

Indeed, the Fourier spectrum gives the energy distribution of the signal in the frequency domain evaluated over the entire time interval:

$$P_{xx}(f) = |\hat{x}(f)|^2 \tag{2}$$

An attempt to deal with transient series is the windowed Fourier transform, which performs the Fourier transform on a sliding segment of the entire time series. However, according to [28], due to the aliasing of high and low frequency components that do not fall within the frequency range of the window, the windowed Fourier transform is inaccurate for time–frequency localization of transient features.

Wavelet analysis is based on the idea of stretching and compressing the window of the windowed Fourier transform, according to the frequencies to be localized, thus allowing the definition of the scales of interest in time and frequency domains. While the Fourier transform uses trigonometric functions as basis, the bases of wavelet transforms are generated through dilations and translations of a single function named wavelet, $\psi(t)$ with finite energy and a zero average.

The continuous wavelet transform (CWT) of a function $x(t)$ is given by:

$$\tilde{X}(a,b) = \int_t x(t) \psi_{a,b}(t) dt \quad a,b \in R \tag{3}$$

where the functions $\psi_{a,b}(t)$ are the wavelet basis. The scale and position parameters a and b are related to the frequency and time of the analyzed function. The respective wavelet spectrum is the matrix of the squared wavelet coefficients:

$$P_{xx}(a,b) = |\tilde{X}(a,b)|^2 \tag{4}$$

While the Fourier power spectrum, Eq. (2), gives the energy for each frequency over the entire time domain, in the wavelet spectrum, Eq. (4), the energy is related to a given time and scale (or frequency). This characteristic of the wavelet transform allows the representation of the distribution of the energy of a given signal over time and frequency domains. This representation is also called spectrogram.

The continuous wavelet spectrum gives a general view of the energy distribution of a signal over time and scale and, due to the inherent redundancy of the CWT, is able to emphasize the signal singularities. As turbulence analysis results are usually presented as frequency functions, the correspondence between frequency and scale should be done. For the present work the correspondence was obtained, according to [29], by:

$$f = \frac{F_\psi \cdot Fs}{a} \tag{5}$$

where F_ψ is the pseudo frequency of the wavelet and Fs is the data acquisition frequency of the signal.

Although the CWT is very useful to pick out some features of the signal, it is a redundant representation, this leads to the discrete wavelet transform (DWT) which deals with dyadic scales, and is given by:

$$\tilde{X}(j,k) = \sum_t x(t)\psi_{j,k}(t) \quad j,k \in \mathrm{I} \tag{6}$$

where the scale and position coefficients (j, k) are dyadic sub samples of (a, b).

The DWT can be regarded as a sub sampling of the CWT [30], with no loss of information.

The discrete wavelet spectrum is defined by:

$$P_{xx}(j,k) = |\tilde{X}(j,k)|^2 \tag{7}$$

The Fourier transform of a finite series gives only a finite number of coefficients, depending on the length of the time series, and therefore neglects the coefficients related to the higher frequencies. Nevertheless, these frequencies must be filtered at the acquisition process, to prevent aliasing. In the wavelet transform of a finite series, the length of the series also restricts the number of computable coefficients but, unlike the Fourier transform, the remaining coefficients are related to the lower frequencies, including the mean value of the signal, and cannot be disregarded. In practice, the DWT of a series with more than 2^J elements is computed for $1 \leqslant j \leqslant J$, being J a convenient arbitrary choice. The remaining part of the signal, containing the mean values for a scale J, is given by:

$$\tilde{X}(J,k) = \sum_t x(t)\phi_{J,k}(t) \tag{8}$$

where $\phi(t)$ is the scaling function associated to the wavelet function. Then, any discrete time series with a sampling frequency Fs can be represented by:

$$x(t) = \sum_k \tilde{X}(J,k)\phi_{J,k}(t) + \sum_{j \leqslant J}\sum_k \tilde{X}(j,k)\psi_{j,k}(t) \tag{9}$$

where the first term is the approximation of the signal at the scale J, which corresponds to the frequency interval $[0, Fs/2^{J+1}]$ and the inner summation of the second term are details of the signal at the scales j $(1 \leqslant j \leqslant J)$, which corresponds to frequency intervals $[Fs/2^{j+1}, Fs/2^j]$

The DWT is computed via the pyramid algorithm [31]. A modification of this algorithm yields the so called discrete wavelet packed transform (DWPT), where each detail series is wavelet transformed in two series, with respectively lower and upper half bandwidth frequency interval. As well as the discrete wavelet transform (DWT) is a judicious sub sampling of the CWT, dealing with dyadic scales, the discrete wavelet packet transform (DWPT) is essentially a modification of the DWT, in order to obtain the decomposition of the signal in successive intervals of equal bandwidth and is done by

$$\tilde{X}(j,m,k) = \int_{-\infty}^{\infty} x(t)\psi_{j,m,k}(t)dt \tag{10}$$

where the scale and position coefficients (j, $k \in$ I) are dyadic sub samples of (a, b) and m is the modulation parameter

In the DWPT, for each level j one can obtain 2^j successive intervals of equal bandwidth. This recursive transformation of detail series is represented in a binary tree. Any admissible binary tree can be chosen for the representation of the signal in the wavelet space, with frequency intervals of unequal bandwidths, according to the analysis to be done. An admissible tree is any binary tree where each node has either 0 or 2 branches.

The discrete wavelet packet spectrum is defined by:

$$P_{xx}(j,m,k) = |\tilde{X}(j,m,k)|^2 \tag{11}$$

where the values assumed by the parameters j, m, and k must follow an admissible tree.

The transient velocity signal was analyzed using wavelet transforms. The CWT was used to construct the continuous wavelet spectrum. The DWPT was used to decompose the measured signal in wavelet approximations at successive frequency intervals [23]. Mathematical tools were developed using the Matlab® software.

3. Experimental technique

The test apparatus, shown schematically in Fig. 1, is a 1370 mm long rectangular channel, with 146 mm height and a width of 193 mm. Air, at room temperature, is the working fluid, driven by a centrifugal blower, passed by a diffuser and a set of honeycombs and screens, before reaching the measurement location with about 1% turbulence intensity. Blower speed is controlled by a frequency inverter. The cylinder has a diameter of 32 mm and is rigidly mounted in vertical position inside the channel. The incidence angle of the flow on the cylinder is 90°. Upstream the measurement location, a Pitot tube is placed at a fixed position to measure the steady reference velocity of the experiments. The geometric blockage ratio is 16.5%.

Velocity and velocity fluctuations were measured by means of a DANTEC StreamLine constant temperature hot wire anemometer and single straight probes. One probe was mounted close to the Pitot tube to measure the reference velocity whereas the other was positioned at the wake, 100 mm downstream the cylinder.

Simultaneous data acquisition of wake and reference velocities were performed with a 12 bit Keithley DAS-58 A/D-converter board with a sampling frequency of 800 Hz and a low pass filter at 300 Hz.

Two distinct experiments were performed. For the first one, the data sets were acquired in steady state flows at regularly spaced velocity values. The velocities were adjusted by means of the frequency inverter coupled to the blower. The second experiment was done in a transient flow. For the transient flow experiment, the settings of the frequency inverter were adjusted in order to promote a 10 s constant acceleration interval (by means of a linear growing of the frequency of the blower from 0 to 60 Hz), 12 s of constant frequency (and steady state flow) and a 5 s constant deceleration interval. Due to the blower inertia, the deceleration interval extended to nearly 10 s and the variation of the average velocity was not exactly linear, as shown in Fig. 2a, for the interval after 25 s. The arrangement enabled recording both transients at

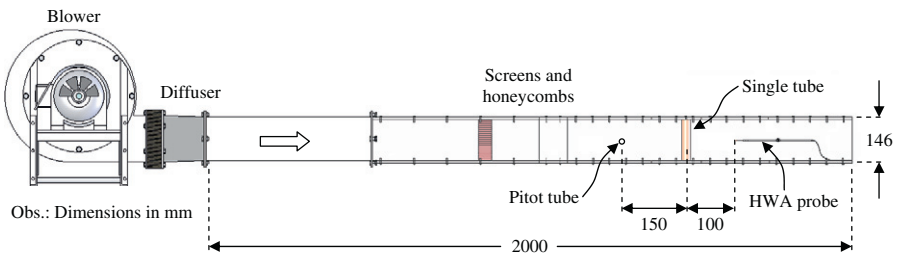

Fig. 1. Schematic view of the test apparatus.

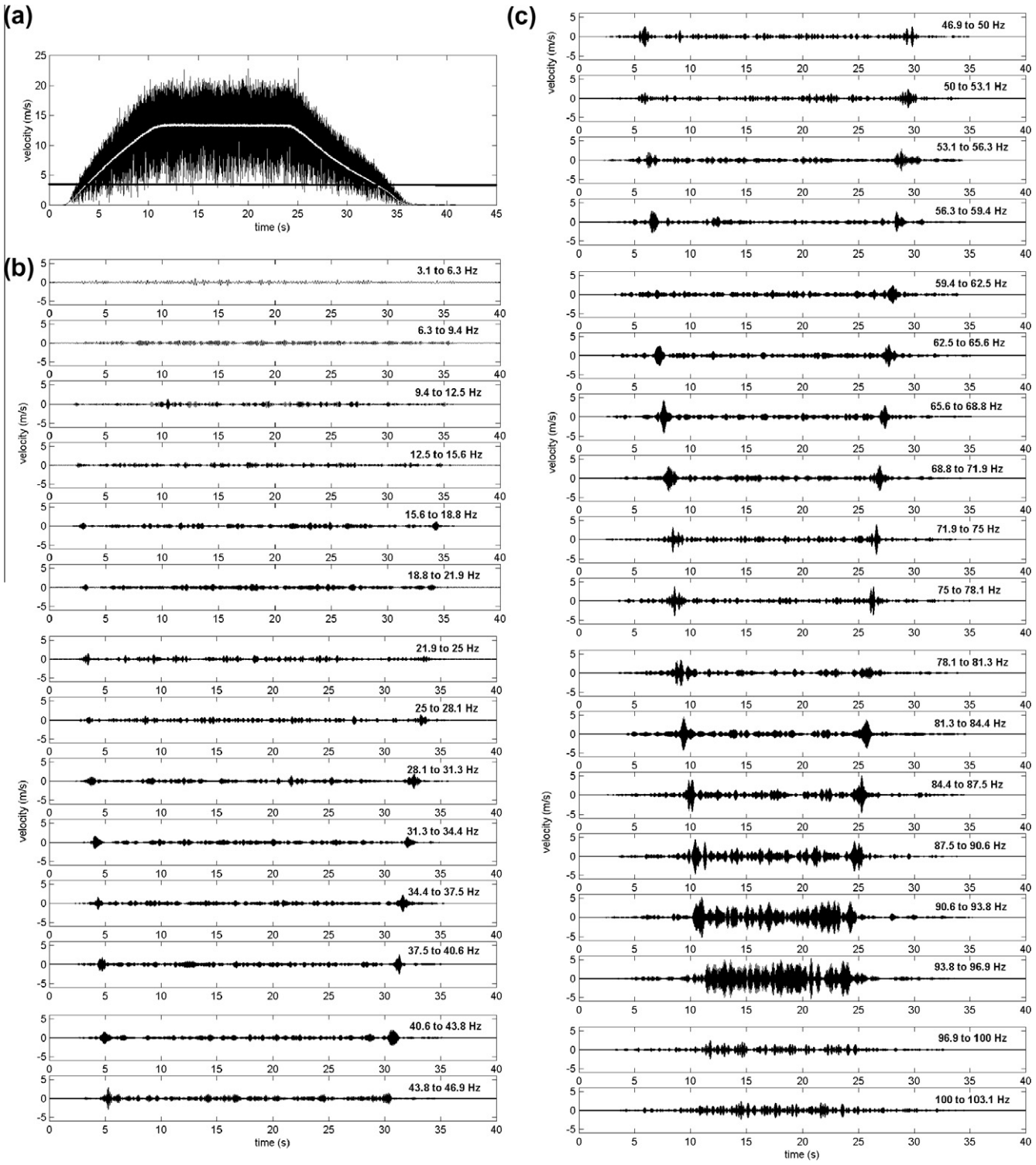

Fig. 2. (a) Transient wake velocity and corresponding reference velocity (in white); (b) and (c) reconstruction of the transient wake velocity for successive frequency intervals with 3.1 Hz bandwidth.

the same acquisition and ensured the repeatability of the accelerating and decelerating processes.

Analysis of uncertainties of the results showed that the error in the determination of the flow velocity varies from 4.4% for the lowest velocities to 0.3% for the highest ones. The error in the determination of the shedding frequencies varies from 1.1% for the lowest frequencies to 0.1% for the highest ones.

4. Results

The first step of the experiment was the determination, via Fourier analysis, of the shedding frequency and the corresponding Strouhal number, defined with the diameter and the approaching velocity, for each one of the signals acquired in steady state, with different approaching velocities. The highest shedding frequency

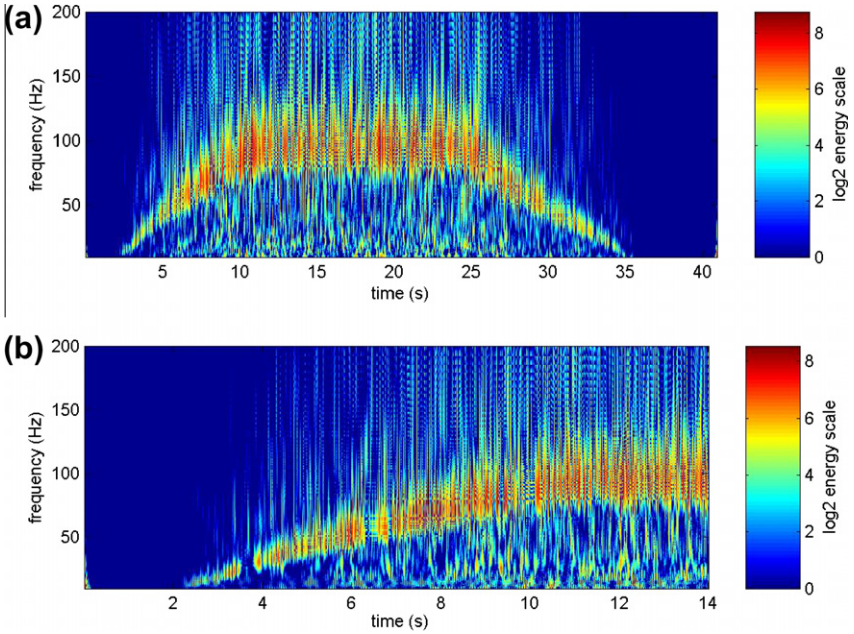

Fig. 3. (a) Wavelet spectrum of the wake velocity data; and (b) detail showing the accelerating part.

was 94 Hz and the corresponding Strouhal number was 0.222. This is an acceptable result taking into account the high value of blockage ratio of the present work, the uncertainty in the velocity measurement and the bandwidth of the frequency determination. These results were compared with the results of the second experiment, whose analysis is described in the sequence.

The DWT decomposes the signal in successive approximation and detail sets of coefficients. The scale of the data of each set is twice as large as the preceding one. The dyadic resultant frequency bandwidths are too large to give any quantitative detailed information about the evolution of the wake frequencies along time. Therefore, the DWPT was applied to the transient signal (second experiment). Several wavelet functions were applied and the DB-20 [32] was chosen as presenting the best relation visualization–localization for the present case. In Fig. 2, the first 7th level reconstructed series, up to 103.1 Hz, are shown. The series show the velocity fluctuations at successive frequency intervals, each with the same bandwidth of 3.1 Hz.

For each frequency interval, departing from 9.4 Hz and following the series until 93.8 Hz, two localized jumps of amplitude are observed, showing the presence of the wake at the corresponding frequency and at the time locations related to acceleration and deceleration periods. At the next frequency interval, from 93.8 to 96.9 Hz, the increase of amplitude, which begins near the onset of steady state velocity, holds until the beginning of the deceleration, denoting the steady state wake. The Fourier spectrum of the steady part of the signal gives 94 Hz as the vortex shedding frequency. At frequencies above 96.9 Hz, the sequence of increased amplitudes disappears and only small amplitudes remain evenly distributed along time. For frequencies lower than 9.4 Hz, the amplitudes corresponding to the vortex shedding are not visible, due to the low energy level of the wake.

For the computation of the continuous wavelet spectra of velocity signals in the wake, Morlet wavelet functions [32] were used. The choice of the Morlet function among others was done taking into account the visibility of the results as shown in [17,19]. For visibility, Fig. 3 shows only the part of the spectrum comprising the frequencies of the wake (1–200 Hz). In the logarithmic energy scale, the minor energy levels were truncated to enhance the visibility of the wake feature, but the major levels were not truncated. Fig. 3a is therefore an energy overview of the experiment, showing the accelerating and decelerating wakes and, between them, the wake in the time interval where the velocity of the blower was constant. Fig. 3b presents the details of Fig. 3a concerning the accelerating period of the experiment. One can see more clearly that the energy level at the beginning of the experiment is very weak in comparison with the whole signal, being barely observed. Besides, Fig. 3b shows the presence of intermittencies on the wake from 3.5 to 3.8 s, as well as from 6.5 to 6.7 s. This intermittence occurs also in the steady part of the signal e.g. between 9.7 and 10.1 s. In these locations, the energy value in the corresponding shedding frequency is comparable to the energy of the remaining scales. This fact is also observed in the decelerating process (Fig. 3a). Therefore, the shedding process is not continuous along time, rather it is intermittent and the shedding frequencies do not follow exactly a linear path. Indeed, they seem to wander around that path, with fluctuations of energy levels as well. It is remarkable that, also in the interval with constant velocity, the frequency and the energy of the wake fluctuate around the mean value.

The energy and frequency fluctuations of the wake are not observable at Fourier analysis that presents only average values. The same occurs with the average values of time averaged wavelet spectra, obtained by integration over a time interval. The time averaged wavelet spectra for time intervals of 0.38 s, computed from the same data of Fig. 3, are displayed in Fig. 4 along with the Fourier spectra of the steady state signals. The evolution of the energy of the transient wake with time is observed and can be contrasted with the spectral results obtained for the sequence of steady state signals. The velocity indicated at each spectrum is the average steady incident velocity for the steady state signals, and is the mean value of the incident velocity at the time interval for the transient signal. The broad overview of the shedding frequencies evolution is similar for both experiments. The smoother aspect of the wavelet spectra is due to the evolution of the wake during the time interval of integration.

Frequencies in problems involving steady fluid flow impinging on a structure are represented usually in non-dimensional form as Strouhal number, defined for a cylinder with the diameter and

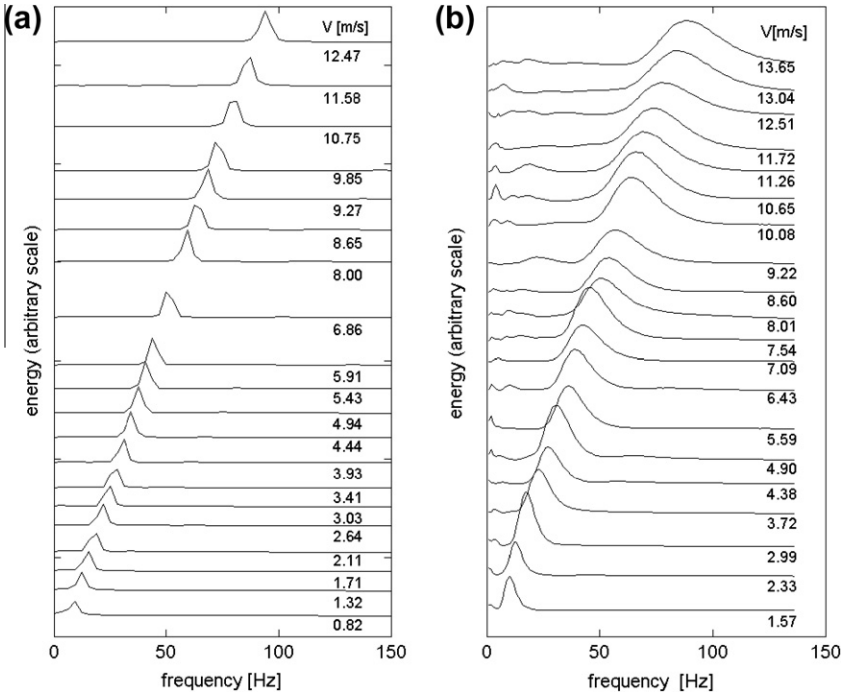

Fig. 4. (a) Fourier power spectra of the steady state signals; and (b) Time mean wavelet spectra, given for each 0.38 s time interval, computed from data of Fig. 3.

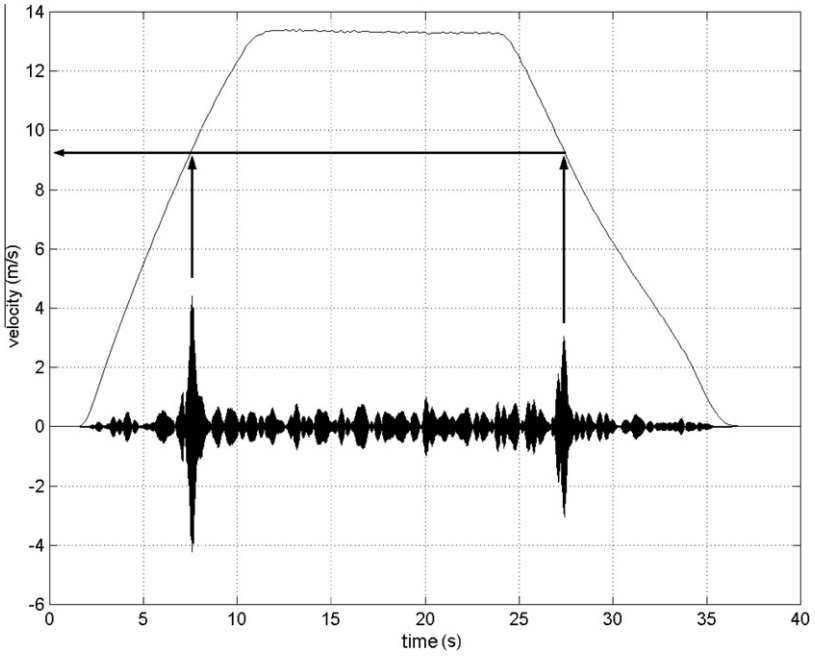

Fig. 5. Time localization, for a chosen frequency interval, of the transient vortex shedding and respective transient incident velocity.

the approaching velocity. A transient Strouhal number can be similarly defined with the instantaneous mean approaching velocity and the mean frequency of the interval, $\bar{f}(t)$. The instantaneous mean approaching velocity was obtained from the first reconstructed 7th level set of the DWPT of the reference velocity signal corresponding to a low pass filter of 3.1 Hz. The instantaneous mean frequency is the mean frequency of each 7th level reconstructed signal of the DWPT.

For each reconstructed series, corresponding to a given frequency interval, the two localized jumps of amplitude denote the time position of the wake at acceleration and deceleration process and can be associated with the respective mean approaching velocity to compute the transient Strouhal number. Fig. 5 shows an example of the graphical scheme used for determining the mean frequency and the corresponding mean approaching velocity. The vortex shedding contributes to the uncertainties in the determination of the transient Strouhal number, since it does not occur at a single distinct frequency; instead, the shedding frequency varies along time in a narrow interval of frequencies within a range of amplitudes [33], as can be observed in Fig. 3b. Heisenberg's uncer-

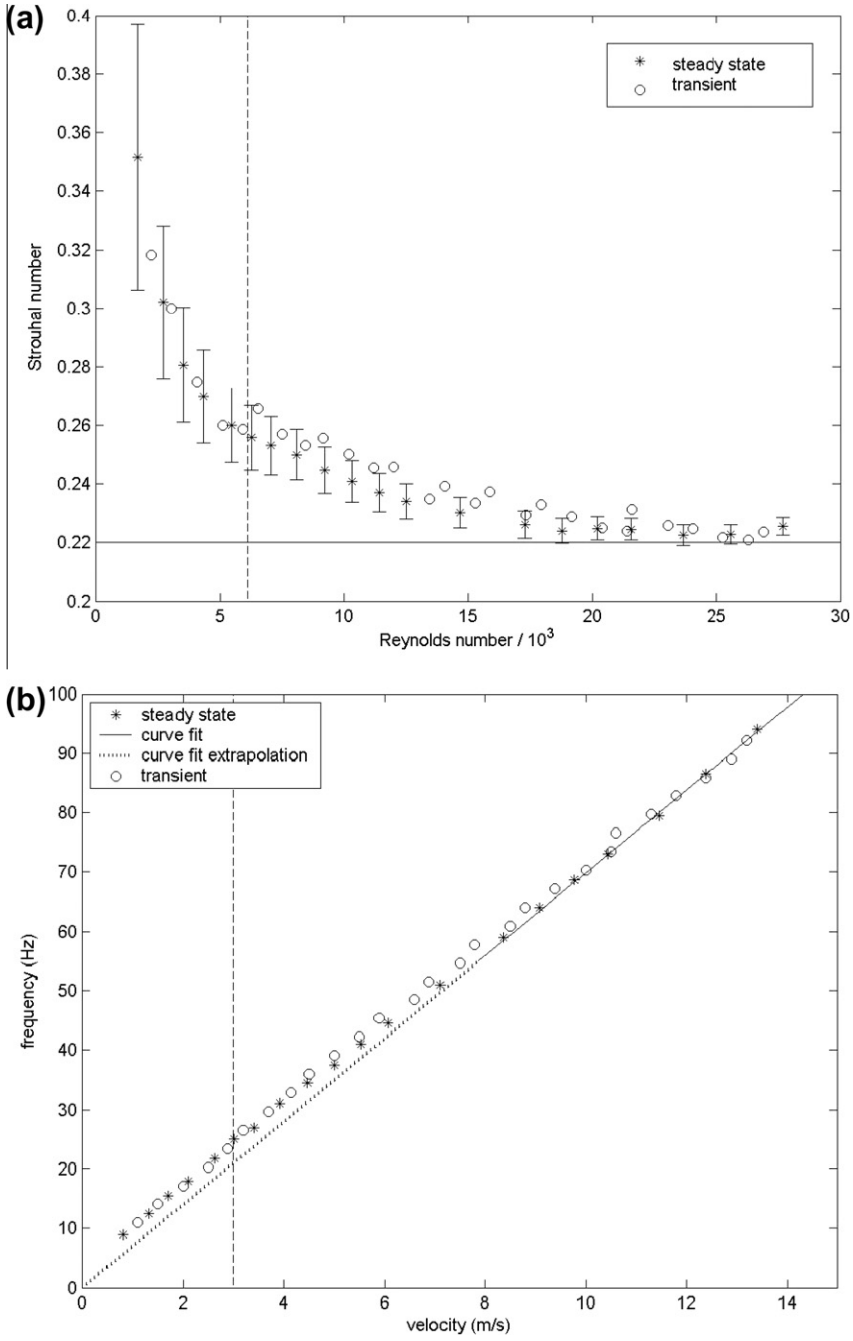

Fig. 6. (a) Strouhal numbers S(t) as a function of Reynolds number; and (b) transient frequency and approaching velocity corresponding to Strouhal and Reynolds numbers of (a). In both figures, the dotted vertical lines indicate the lower limit of reliability of the velocity measurements.

tainty principle limits the use of a higher-level DWPT with a narrower frequency bandwidth, because the time localization of the wake features becomes less accurate [31].

Fig. 6a shows the values of the transient Strouhal numbers S(t) computed for each series of Fig. 2, as a function of instantaneous Reynolds number. They are plotted along with the results obtained by Fourier analysis of the data acquisitions in steady state flows. The error bars were presented for the Strouhal numbers obtained from the Fourier analysis of the steady state signals. For the transient signal, albeit presenting good results, it is difficult to evaluate the uncertainties of the graphic scheme illustrated in Fig. 5, the uncertainty principle playing the main role in the problem. The results for both transient and steady state signals show good agreement, indicating that the transient wake behaves as a succession of steady states. They also allow concluding that: (a) the wavelet analysis performed in this work is effective for the identification of transient features of the signal and (b) the accuracy of the time–frequency localization of the wavelet transform is sufficient to perform such analysis, considering the limitations imposed by the uncertainty principle.

The unexpected strong increase of the Strouhal numbers at lower Reynolds numbers observed in the present results, which is not in agreement with the traditional results shown in [33,34], can be attributed to the high blockage ratio of the test section. For Reynolds numbers greater then 1.8×10^4, the Strouhal number remains almost constant. This agrees with the results of West and

Apelt for Reynolds numbers between 2.5×10^4 and 15×10^4 [25]. According to Žukauskas [35], depending on the position, the deviation of the flow due to the blockage can increase the velocity around the cylinder up to 80%. Contribution of the higher uncertainties in velocity measurements below 3 m/s and of the bandwidth on the frequency determination can also contribute to the higher values of the Strouhal numbers below Re = 6000. Reducing the bandwidth to improve the frequency resolution of Fourier spectra do not contribute to the improvement of the results, while the mean statistical errors are increased. The reduction of the bandwidth in wavelet analysis is limited by Heisenberg's uncertainty principle [31], as mentioned before.

Nevertheless, the bias of the results is the same for both steady state and transient measurements and similar values can be expected. Indeed, the wavelet and Fourier results agree also at this low range.

The plot of velocity as a function of the frequency, Fig. 6b, shows the linear behavior that corresponds to the definition of the Strouhal number. The continuous line represents the linear fit of the steady state results considering only velocities above 8 m/s. Dotted line is the curve fit extrapolation until axes origin. Experimental data points below this velocity value lie above the curve, confirming the increasing values of Strouhal number for the lower Reynolds number range in Fig. 6a.

The present results are complementary to those of Refs. [25–27], confirming that, for blockage ratio of 16.5% and $Re < 2.5 \times 10^4$, the Strouhal numbers are strongly increased as the Reynolds number is reduced.

5. Concluding remarks

In this work, a discrete wavelet analysis was used to study the transient behavior of the known phenomenon of a wake behind a circular cylinder submitted to a turbulent flow.

Steady state phenomena are a particular case of the transient general rule in nature. In engineering applications the steady state assumption is very useful and feasible in most situations. However, some features of the phenomena may remain unnoticed, so the use of a straightforward methodology of signal analysis that deals with the transient features and is related with the usual Fourier analysis was proposed and presented.

In the present work, the transient flows were obtained by simply turning on and off the frequency inverter who controlled the blower, thus controlling the duration of the accelerating and decelerating processes.

Comparison of the results of the transient Strouhal number with a succession of steady states demonstrates that the wavelet analysis of the transient signal, obtained at once, from only one data acquisition, has a close agreement with the results of the set of data acquisitions at steady flows, with the velocity of the blower adjusted at regularly spaced values. This yields the conclusion that the analysis of field measurements data can be considerably improved by the use of wavelet techniques. The use of wavelet analysis is also a time saving technique which can improve the probability of stable environmental conditions at the entire time interval of the experiment.

The role of the blockage in experimental apparatus and also in some practical applications can not be neglected. Despite of the uncertainties of the results for very low Reynolds numbers for both Fourier and wavelet analysis, the departure from the usual values of the Strouhal numbers obtained in the present work is noticeable and suggests that blockage should be carefully considered in the analysis of engineering processes and experiments. The results of the present work complement [25–27], confirming that, for high blockage ratios, the Strouhal number increases at low Reynolds numbers.

Acknowledgements

Authors gratefully acknowledge the support by The National Council for Scientific and Technological Development (CNPq), Ministry of Science and Technology (MCT), Brazil.

References

[1] V. Strouhal, Über eine besondere art der tonerregung, Ann. Phys. Chem. 5 (1878) 216–251. New series.
[2] H. Bénard, Formation périodique de centres de giration à l'arrière d'un obstacle en mouvement, C.R. Acad. Sci. 147 (1908) 839–842.
[3] H. Bénard, Etude cinématographique des ramous et des rides produits par la translation d'un obstacle, C.R. Acad. Sci. 147 (1908) 970–972.
[4] D. Brika, A. Laneville, Wake interference between two circular cylinders, J. Wind Eng. Ind. Aerodyn. 72 (1997) 61–70.
[5] C. Lin, S.C. Hsieh, Convection velocity of vortex structures in the near wake of a circular cylinder, J. Eng. Mech. – ASCE 129 (2003) 1108–1118.
[6] S.J. Xu, Y. Zhou, R.M.C. So, Reynolds number effects on the flow structure behind two side-by-side cylinders, Phys. Fluids 15 (5) (2003) 1214–1219.
[7] S. Ozono, Vortex suppression of the cylinder wake by deflectors, J. Wind Eng. Ind. Aerodyn. 91 (2003) 91–99.
[8] S.J. Lee, S.I. Lee, C.W. Park, Reducing the drag on a circular cylinder by upstream installation of a small control rod, Fluid Dynam. Res. 34 (2004) 233–250.
[9] M. Ozgoren, Flow structure in the downstream of square and circular cylinders, Flow Measur. Instrum. 17 (2006) 225–235.
[10] C.-C. Chu, Y.-Y. Liao, A quantitative study of the flow around an impulsively started circular cylinder, Exp. Fluids 13 (1992) 137–146.
[11] M.C.H. Hui, A. Larsen, H.F. Xiang, Wind turbulence characteristics study at the Stonecutters bridge site: part I—mean wind and turbulence intensities, J. Wind Eng. Ind. Aerodyn. 97 (2009) 22–36.
[12] M.C.H. Hui, A. Larsen, H.F. Xiang, Wind turbulence characteristics study at the Stonecutters bridge site: part II—Mean wind and turbulence intensities, J. Wind Eng. Ind. Aerodyn. 97 (2009) 48–59.
[13] M. Farge, N. Kevlahan, V. Perrier, K. Schneider, Turbulence Analysis, Modeling and Computing Using Wavelets, in: J.C. Van Den Berg (Ed.), Wavelets in Physics, Cambridge University Press, 1999, pp. 117–200.
[14] H. Mouri, H. Kubotani, T. Fujitani, H. Niino, M. Takaoka, Wavelet analyses of velocities in laboratory isotropic turbulence, J. Fluid Mech. 389 (1999) 229–254.
[15] V. Perrier, T. Philipovitch, C. Basdevant, Wavelet spectra compared to Fourier spectra, J. Math. Phys. 36 (1995) 1506–1519.
[16] M.R. Hajj, H.W. Tieleman, L. Tian, Wind tunnel simulation of time variations of turbulence and effects on pressure on surface-mounted prisms, J. Wind Eng. Ind. Aerodyn. 88 (2000) 197–212.
[17] X. Gilliam, J. Dunyak, A. Doggett, D. Smith, Coherent structure detection using wavelet analysis in long time-series, J. Wind Eng. Ind. Aerodyn. 88 (2000) 83–195.
[18] C. Meneveau, Analysis of turbulence in the orthonormal wavelet representation, J. Fluid Mech. 232 (1991) 469–550.
[19] M.M. Alam, M. Moriya, H. Sakamoto, Aerodynamic characteristics of two side-by-side circular cylinders and application of wavelet analysis on the switching phenomenon, J. Fluids Struct. 18 (2003) 325–346.
[20] M.M. Alam, Y. Zhou, Strouhal numbers, forces and flow structures around two tandem cylinders of different diameters, J. Fluids Struct. 24 (2008) 505–526.
[21] A. Rinoshika, Y. Zhou, Orthogonal wavelet multi-resolution analysis of a turbulent cylinder wake, J. Fluid Mech. 524 (2005) 229–248.
[22] A. Rinoshika, T. Zhou, Y. Zhou, Orthogonal wavelet-decomposed 3D vorticity of a turbulent flow, JSME Int. J. Ser. B 49 (4) (2006) 1149–1155.
[23] M.L.S. Indrusiak, J.V. Goulart, C.R. Olinto, S.V. Möller, Wavelet time frequency analysis of accelerating and decelerating flows in a tube bank, Nucl. Eng. Des. 235 (2005) 1875–1887.
[24] C.R. Olinto, M.L.S. Indrusiak, S.V. Möller, Experimental study of the bistable flow in tube arrays, J. Brazilian Soc. Mech. Eng., São Paulo 5 (2006) 221–229.
[25] G.S. West, C.J. Apelt, The effects of tunnel blockage and aspect ratio on the mean flow past a circular cylinder with Reynolds numbers between 10^4 and 10^5, J. Fluid Mech. 114 (1982) 361–377.
[26] R.W. Davis, E.F. Moore, L.P. Purtell, A numerical–experimental study of confined flow around rectangular cylinders, Phys. Fluids 27 (1983) 46–59.
[27] P. Anagnostopoulos, G. Iliadis, S. Richardson, Numerical study of the blockage effects on viscous flow past a circular cylinder, Int. J. Numer. Methods Fluids 22 (1996) 1061–1074.
[28] C. Torrence, G.P. Compo, A practical guide to wavelet analysis, Bull. Am. Meteorol. Soc. (1998).
[29] P. Abry, Ondelettes et Turbulence, Multirésolutions, Algorithms de Décomposition, Invariance D'échelles, Paris, Diderot Editeur, 1997.

[30] D.B. Percival, A.T. Walden, Wavelet Methods for Time Series Analysis, Cambridge University Press, Cambridge, 2000.
[31] S. Mallat, A Wavelet Tour of Signal Processing, second ed., San Diego, Academic Press, 1999.
[32] I. Daubechies, Ten Lectures on Wavelets, SIAM – Society for Industrial and Applied Mathematics, Philadelphia, 1992.
[33] H. Schlichting, Boundary-Layer Theory, McGraw-Hill, New York, 1979.
[34] R.D. Blevins, Flow-Induced Vibration, second ed., Van Nostrand Reinhold, New York, 1990.
[35] A. Žukauskas, Heat Transfer from Tubes in Crossflow, Advances in Heat Transfer, vol. 8, Academic Press Inc., New York, 1972.